Breaking of Symmetry in Graphene Growth on Metal Substrates

Vasilii I. Artyukhov,[1] Yufeng Hao,[2] Rodney S. Ruoff,[3,4] and Boris I. Yakobson[1,*]
[1]Department of Materials Science and NanoEngineering, Rice University, Houston, Texas 77005, USA
[2]Department of Mechanical Engineering, Columbia University, New York, New York 10027, USA
[3]Center for Multidimensional Carbon Materials, Institute for Basic Science (IBS), Ulsan 689-798, Republic of Korea
[4]Department of Chemistry, Ulsan National Institute of Science and Technology (UNIST), Ulsan 689-798, Republic of Korea
(Received 4 September 2014; revised manuscript received 28 January 2015; published 16 March 2015)

In graphene growth, island symmetry can become lower than the intrinsic symmetries of both graphene and the substrate. First-principles calculations and Monte Carlo modeling explain the shapes observed in our experiments and earlier studies for various metal surface symmetries. For equilibrium shape, edge energy variations δE manifest in distorted hexagons with different ground-state edge structures. In growth or nucleation, energy variation enters exponentially as $\sim e^{\delta E/k_B T}$, strongly amplifying the symmetry breaking, up to completely changing the shapes to triangular, ribbonlike, or rhombic.

DOI: 10.1103/PhysRevLett.114.115502 PACS numbers: 61.48.Gh, 81.05.ue, 81.10.Aj

While exfoliation techniques can produce monolayers of graphene [1] and other two-dimensional materials [2] of extraordinary quality [3], their lack of scalability hampers their use in applications. Chemical vapor deposition (CVD) synthesis [4] can address the scalability concern. However, it is difficult to produce graphene samples of quality comparable to exfoliated layers [5], motivating both empirical and theoretical effort to understand and improve graphene growth.

Because CVD involves a solid substrate in contact with graphene, their interaction alters the latter's properties. This influence cannot be described simply as the interaction of a complete graphene crystal with the support. Instead, the relevant processes occur as graphene assembles. Because of the inherent difficulty of observing growth *in situ*, theoretical understanding is indispensable.

Previous study of the morphology of graphene under kinetic or thermodynamic control from an atomistic level [6] was able to predict many observed shapes such as zigzag-edged (slowest growing) hexagons [7–9] or dodecagons with 19.1° (fastest etching) [10] and 30° (equilibrium shape) angles [11]. All these shapes inherit the hexagonal symmetry of graphene. Yet, recurring observations of less symmetric shapes call for a deeper study of the effects of the substrate on the growth of graphene. In this work we reveal how symmetry breaking manifests in graphene growth and results in shapes with lowered (threefold, twofold) symmetry, using Ni and Cu substrates as examples. For the equilibrium shape of graphene on the Ni(111) surface, we show using first-principles calculations how tangential "sliding" breaks inversion symmetry and leads to different atomistic structures at opposite edges of graphene islands, yet the effect on the Wulff shape is rather weak. However, since the growth rates contain the energy terms affected by symmetry in the exponent, we find that under kinetic control, the asymmetry is amplified, causing a qualitative transition from hexagonal (equilibrium) to triangular (growth) shapes. Nucleation statistics, also exponential in the symmetry-breaking strength, can cause strong selection of just one of the two near-degenerate stacking "phases" of graphene. Casting the atomistic insight into a coarse-grained Monte Carlo (MC) model of growth, we explain our observations of broken-symmetry islands on different surfaces of polycrystalline Cu foil.

Typically, graphene is incommensurate with substrates used for CVD growth. Without translational invariance even the most basic concepts such as interface energy and Wulff construction cease to be reliable footholds. Therefore, we first focus on the important special case of Ni(111) substrate [with Co(0001) being essentially analogous], where graphene can stretch by ~1% to accommodate the lattice constant of the metal surface, resulting in perfect epitaxial matching. Since both the (111) surface and graphene have a sixfold rotation axis, it is possible to form an interface that preserves this symmetry. However, it turns out to be unstable with respect to tangential displacements that break the alignment of the C_6 axes producing other stacking phases that reduce the symmetry to threefold (or even twofold). Typically, one sublattice of carbon atoms is on *top* of the upper-layer Ni atoms, and the other is either in *fcc* or *hcp* sites of the Ni lattice, forming two almost-degenerate structures (Fig. 1) that differ only in positioning with respect to the second layer of Ni. Either way, the overall symmetry is triangular rather than hexagonal and graphene sublattices become inequivalent—like in boron nitride [12]. In particular, the six previously degenerate Z edges split up into two triplets, denoted as ∇ and Δ.

We begin with determining the substrate effect on the equilibrium shape of graphene on Ni(111). The edge energy for arbitrary orientation χ can be expressed analytically from basic armchair (A) and zigzag (Z) edge energies [13], accounting for inequivalent Z edges:

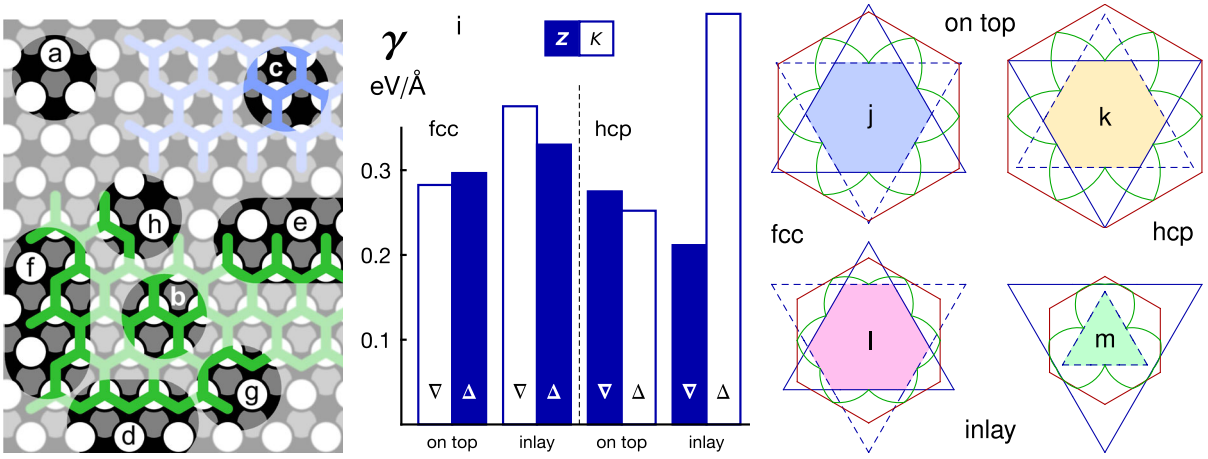

FIG. 1 (color online). (a)–(h) Stacking of graphene on Ni(111) surface. The substrate (a) is shown in white, gray, and black according to the depth. Graphene is shown in green (b) for *fcc* and blue (c) for *hcp* stacking. Graphene edges: (d) hexagonal zigzag Z, (e) Klein K, and (f) armchair (showing the A5' reconstruction [6]). Edge kinks k are shown on Z (g) and K (h) edges. (i) Zigzag edge energies computed with density functional theory for different stacking (*fcc*, *hcp*), direction (∇, Δ), and edge structure (Z, K) in the on-top and inlay graphene arrangement with respect to the top Ni layer. The bar width is 0.04 eV/Å or 0.1 eV per edge unit cell, corresponding to $\sim k_B T$ at typical growth temperatures (~1000 K). (j)–(m) Wulff constructions for the respective cases: (green) edge energy $\gamma(\chi)$; blue lines denote (solid) Z and (dashed) K edges.

$\gamma(\chi) = 2\gamma_A \sin(\chi) + 2\gamma_i \sin(30° - \chi)$. Here, χ is the angle with respect to the closest ∇ direction, $i = \nabla$ when $|\chi| \bmod 60° < 30°$, and $i = \Delta$ otherwise. Since the A edge symmetry is not broken by the substrate, γ_A is known from previous work [6], leaving us with just the two zigzag edge energies γ_∇ and γ_Δ to compute. As a consequence of inversion symmetry breaking, not only the energies of ∇ and Δ edges can be different, but the edges can have different ground-state atomistic structures. Using density functional theory computations [14–17] (details in Supplemental Material [18]), we screened a total of 12 possible combinations: 2 for stacking $(fcc, hcp) \times 2$ for direction $(\nabla, \Delta) \times 3$ structures (conventional hexagonal zigzag Z; Klein K [19]; pentagon-reconstructed Klein, e.g., Ref. [20]). The pentagon-Klein reconstruction is always unfavorable. For both stackings, one of the ground-state edge structures is Z, but the opposite side favors K (*fcc*: $K_\nabla \| Z_\Delta$; *hcp*: $Z_\nabla \| K_\Delta$) as *top* C atoms cannot form in-plane bonds with Ni atoms and prefer to be three-coordinated. To determine edge energies in the absence of inversion symmetry, we used a series of increasingly larger triangular islands with only ∇ or only Δ edges [12], by fitting their energies as $E(N) = aN + b\sqrt{N}$, where N is the number of atoms [18]. We considered two scenarios, with graphene flakes on top of the Ni(111) surface or inlaid in the topmost Ni plane [21]. In all cases [Fig. 1(i)] the energies of ∇ and Δ edges are close, except for the inlay-*hcp* case, where it is impossible for the Δ direction to interface with the Ni lattice without a large geometrical strain (hence, the outstandingly high value).

By plotting $\gamma(\chi)$ in polar coordinates [22] [green line in Figs. 1(j)–1(m)], we obtain the Wulff construction. We find that the equilibrium shapes are truncated triangles (lowered-symmetry hexagons), except for the case of inlay-*hcp* stacking. Truncated shapes were recently observed on Ni(111) [23], and according to our calculations, these islands should have Klein edges in three out of six directions. Yet multiple other observations show sharp-cornered triangles on top of the metal surface [21,24], impossible to explain thermodynamically (Fig. 1). This compels us to investigate growth kinetics.

Our "nanoreactor" model of graphene growth [6] is naturally extendable to the case of inversion-inequivalent zigzag edges. We consider only the ground-state edge structures in the on-top scenario. Carbon atoms are added sequentially to the edges (Fig. S1 of the Supplemental Material [18]), yielding the free-energy sequences shown in Fig. 2(a) for *fcc* and Fig. 2(b) for *hcp* stacking. The familiar kink nucleation/flow picture is clearly observed in this plot [6]. In either stacking, the hexagonal Z edge (blue solid line) has a higher free-energy barrier for the formation of a new atomic row than K (blue dashed line): 2.24 versus 1.49 eV for *fcc* and 2.20 versus 1.633 eV for *hcp* (difference $\Delta E \approx 0.6$–0.7 eV). And because the rate of formation of new atomic rows at the edge depends on these energy barriers exponentially, K edges will grow much faster than Z and disappear from the growth shape. The closed-form expression for graphene edge growth velocity [6] can be used (with appropriate modifications to account for broken symmetry) to plot the kinematic Wulff constructions. As seen in Figs. 2(c) and 2(d), the result is a triangle with Z edges, Δ for *fcc* stacking and ∇ for *hcp*.

The essentially equal values of rate-limiting barriers E_Z for the *hcp* and *fcc* stackings predict similar growth rates.

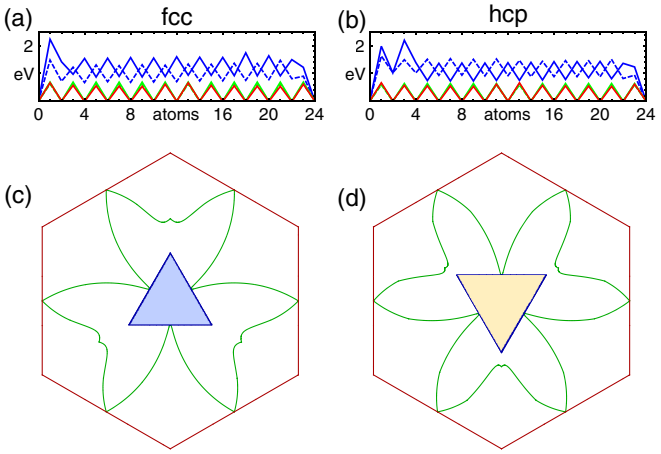

FIG. 2 (color online). Free-energy evolution during graphene edge growth in (a) *fcc* and (b) *hcp* stacking: (blue solid line) Z, (blue dashed line) K, (green line) intermediate, and (red line) armchair edges. Kinematic Wulff constructions for (c) *fcc* and (d) *hcp* stackings: (green line) polar plot of edge growth velocity, (red line) velocity of armchair edges, (blue line) velocity of Z edges. K edges are absent from the construction. The temperature is set high (0.3 eV) in order to "compress" the plots in the radial dimension.

However, to assess their relative abundance one also needs to consider nucleation [25]. Based on the edge energies and difference between *fcc* and *hcp* 2D bulk energies (~0.03 eV/atom from the computations), the free energy of an island can be expressed as a function of its area (number of atoms), $G = (\varepsilon - \mu)N + c\gamma\sqrt{N}$, where ε is the 2D "bulk" energy of the respective graphene phase, μ is the chemical potential, γ is the edge energy, and c is a form factor to discriminate between triangles and hexagons (which we approximate as perfect). Figure 3 shows free-energy $G(N)$ plots for the two "phases" at a chemical potential bias of $\mu - \varepsilon_{fcc} \equiv \Delta\mu = 0.3$ eV for the [3(a)] inlay and [3(b)] on-top scenarios. In the former scenario [3(a)], despite the triangular shape of *hcp* domains, low edge energy yields a much lower nucleation barrier—by 1.54 eV in this example. This leads to a nucleation rate difference $e^{(G^*_{hcp} - G^*_{fcc})/k_BT} \sim 10^6$ in favor of the higher-energy *hcp* phase. Here again exponentiation greatly amplifies the symmetry-breaking effect (compared to the ratio of γ which is only ~1.5). While the growth shapes of the two phases are oppositely oriented [Figs. 2(c) and 2(d)], selective nucleation eliminates one of the two possibilities. This explains the recent observations of co-oriented graphene triangles on Ni(111) [26].

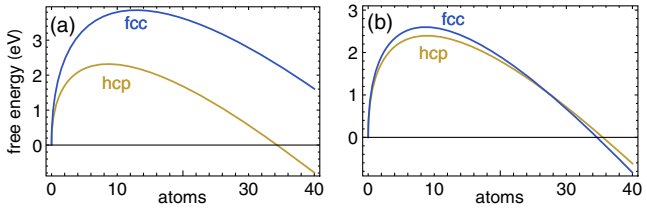

FIG. 3 (color online). Free energy as a function of number of atoms in an island ($\Delta\mu = 0.3$ eV) for (a) inlay and (b) on-top scenarios.

In contrast, for graphene islands on top of the surface, the nucleation barrier difference is merely on the order of k_BT [Fig. 3(b)], implying weak if any selectivity (the stacking preference is reversed around $\Delta\mu = 0.18$ eV). Indeed, both phases were identified via characteristic "translational grain boundary" defects [27] and by direct observations [28].

While Ni(111) provides a convenient system for atomistic analysis, symmetry-breaking effects are equally important for other substrates without perfect epitaxy with graphene, the foremost being copper. Figure 4(a) presents a scanning electron microscope image of graphene islands on a Cu foil. The growth was carried out in a tube furnace CVD system, similar to previous work [9]. For this sample we used an oxygen-free Cu substrate with 0.1 torr H_2 pressure and 10^{-3} torr methane pressure. The growth temperature was 1035 °C and the growth time was 20 min. Several Cu grains are seen, with many graphene islands (dark) on each. Even though all graphene islands grew simultaneously at the same conditions, we see two distinct shape classes. Nearly all islands are hexagonal, but some are almost perfect while others are elongated. All islands on a single Cu grain belong to the same class (except for cases with several islands colliding within the same grain or across the boundaries [29]). Furthermore, graphene islands on each grain are aligned, which is especially noticeable for elongated islands. The density

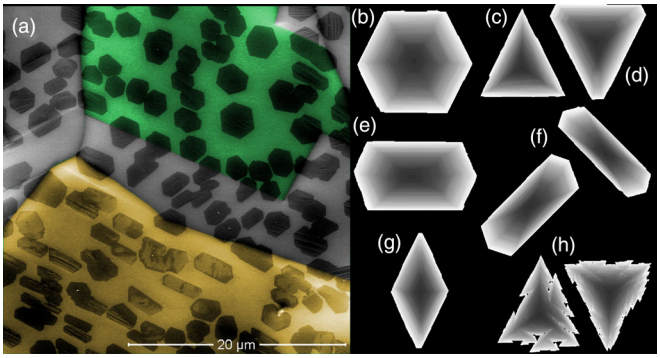

FIG. 4 (color online). (a) Scanning electron microscopy image of graphene grains on a polycrystalline Cu foil with two largest grains highlighted in color. (b)–(h) Monte Carlo modeling of growth: (b) isotropic kinetics, Cu(111); (c) triangle with a 10^3 ($7k_BT$) difference between growth probabilities for ∇ and Δ directions, representing Ni(111); (d) triangle with a 10^1 ($2k_BT$) $\Delta:\nabla$ probability ratio; (e) two slow directions, representing the rectangular Cu(110) surface; (f) two slow directions with two degenerate orientations, Cu(100); (g) same as (e) but with two fast directions; (h) calculations with diffusion. All simulations were run for 30 000 steps. Brightness represents time (lighter cells are more recently added).

of islands and their size is similar between the grains. This suggests that the basic underlying mechanisms in their growth are the same, and the shape difference is determined by subtle differences between crystallographic surfaces of Cu. Indeed, electron backscatter diffraction studies established that hexagonal domains form on Cu(111), while elongated domains grow on Cu (100) or (110) [9,30].

To understand the shapes in Fig. 4(a) we consider the symmetry of the graphene + Cu system. Though the (111) surface is triangular, translational incommensurability of the lattices means that a growing edge will have a different positioning with respect to the underlying Cu atoms at different times, and on average, the symmetry-breaking effects will compensate. Interestingly, this precludes the sliding mode of symmetry breaking [as in Ni(111)] and restores the C_6 symmetry for the composite system. For rectangular (110) and square (100) surfaces, two parallel graphene edges should align with one of the orthogonal basic crystallographic directions of the surface, but the other four edges will remain misaligned with the substrate. Thus, the six edges will be split in two sets of two and four (unlike three and three on Ni). During kink-flow growth, incommensurability of edges with the underlying substrate will again be averaged out, but this time the averaging will differ between the families. Again, the rotational symmetry of graphene islands is reduced to the common divisor of 6 and 2 or 4, respectively, i.e., C_2.

Building on the understanding of how the substrate modulates the growth velocities in different directions, one can model this and other possibilities using coarse-grained MC simulation as follows. Graphene is represented by a triangular lattice (nodes are hexagon centers), starting with a single occupied point. At each time step, all vacant cells with occupied neighbors are classified either as Z sites (three occupied neighbors along a straight line) or k (kink; armchair edge is an "array of kinks" [31]). The relative probability P of addition to a Z site (nucleation of a new atomic row, $P \equiv P_Z/P_k \sim \exp(E_k - E_Z)k_BT$ in the atomistic calculations) is the input parameter. Probabilities of all sites form a distribution that is sampled to determine the next site to be occupied, and the process is iterated. As a result, we obtain the shape in Fig. 4(b), which is the familiar graphene hexagon frequently observed on Cu(111) [7,9], liquid Cu [8], and in Fig. 4(a), in agreement with the nanoreactor model predictions for isotropic substrates [6].

Recalling our analysis of growth kinetics on Ni (Fig. 2), the essential physical insight that explains triangular growth shapes is the difference between probabilities to initiate a new row on Z versus K edges. Our MC model can naturally capture this with two independent parameters for two inequivalent crystallographic orientations of Z edges, P_∇ and P_Δ. Figure 4(c) shows the sharp triangle from a run with $P_\Delta/P_\nabla = 10^{-3}$, corresponding to our first-principles results for ΔE. Only Δ edges are present, and it is in perfect agreement with the analytical kinematic Wulff shape of Fig. 1. Figure 4(d) shows the truncated triangle produced in a run with $P_\nabla/P_\Delta = 10^{-1}$, barely showing any Δ edge fragments. Thus, six-sided shapes are only possible when the growth barrier difference is small, $|E_\nabla - E_\Delta| \lesssim 2$–$3k_BT$, or no more than 0.2 eV for typical graphene CVD conditions, which is a rather close coincidence.

For rectangular surfaces such as Cu(110) or Ge(110) [32], or twofold-symmetric stackings on Ni(111), two input probabilities are again needed, now for the two "horizontal" and four "diagonal" directions, $P_=$ and $P_{\langle\rangle}$. Typically one would expect the edges that are aligned with close-packed surface "grooves" to grow slower, resulting in $P_= < P_{\langle\rangle}$. This produces elongated shapes such as Fig. 4(e), closely resembling the high aspect ratio islands in Fig. 4(a). Cu(100) is similar, but there are now two orthogonal close-packed directions for long graphene edges to align with. This will produce two rather than one preferred alignment at a 90° angle with each other within the same Cu grain [Fig. 4(f)], as observed experimentally [30,33]. Finally, if $P_= > P_{\langle\rangle}$, the shape shown in Fig. 4(g) results.

It is remarkable how a simple MC model informed by atomistics allows a unified description of Ni(111), all surfaces of Cu (including liquid), and pretty much any metal surface without an epitaxial match with graphene just based on its symmetry. It can similarly be applied to model any other graphenelike material with inequivalent sublattices, such as boron nitride [34,35] or transition metal dichalcogenides. By the same token, growth units larger than hexagons [36] can be treated. Going even further one can emulate diffusion in this model. This is achieved by making the growth probabilities depend not only on site type, but also on the number of unoccupied cells within some distance. Edges of protrusions have better access to feedstock supply at the free catalyst surface, producing diffusion instabilities. This refinement reproduces sawtooth patterns seen on the edges of metal chalcogenide islands [37,38] with a characteristic dendritic but not fingerlike morphology [Fig. 4(h)], reminiscent of the Sierpinski fractal.

In summary, the symmetry of emergent carbon islands reflects not the symmetry of graphene *per se* but rather the combined symmetry of its stacking on a substrate surface, which generally is lower than either graphene (hexagonal) or the surface (hexagonal, square, rectangular, etc.). On epitaxially matched surfaces such as Ni(111) or Co(0001), the symmetry-breaking effect is particularly apparent at the edges, resulting in different ground-state structures (Z versus Klein) for different directions (∇, Δ), and causing equilibrium shapes with a (typically mild) violation of inversion symmetry. However, in kinetics, the symmetry-lowering interactions become exponentially amplified as $\sim \exp(-E/k_BT)$, and Klein edges grow much faster than Z, resulting in triangular growth shapes with only Z edges.

Similarly, exponentiation can make symmetry effects strongly pronounced in nucleation, so that edge energy differences can play a decisive role in selection of the graphene-Ni(111) stacking. We apply this insight to growth on Cu, where different graphene island morphologies are concurrently observed on different crystalline grains of the same foil, using a Monte Carlo growth model that draws upon our Ni(111) analysis but can be tuned to any substrate symmetry, commensurate or incommensurate with graphene, crystalline, or liquid. Since crystal symmetry of the substrate dictates both the shape of islands and their alignment, single-crystalline substrates offer better control over both the morphology of graphene islands and grain boundaries in the resulting films. This improved understanding of the role of substrate symmetry in graphene growth is crucial for improving the quality [4] or engineering grain boundaries [5] in CVD graphene.

This work was supported by the Department of Energy, BES Grant No. DE-SC0012547 and in part (Klein edge analysis) by the AFOSR Grant No. FA9550-14-1-0107. Y. H. and R. S. R. appreciate support from SWAN-NRI, and R. S. R. also from IBS-R019-D1. We thank S. Hofmann (Cambridge University) for discussions.

Note added in proof.—Recent atomic-resolution STM imaging of graphene edges on Ni(111) revealed, in addition to Z and K edges, (2×1) superstructures interpreted as pentagonal-Klein edges stabilized by hydrogen at low temperatures [39] and as pentagon-heptagon reconstruction [40]. K edges were also observed on Co(0001) [41].

*biy@rice.edu

[1] K. S. Novoselov, A. K. Geim, S. V. Morozov, D. Jiang, Y. Zhang, S. V. Dubonos, I. V. Grigorieva, and A. A. Firsov, Electric field effect in atomically thin Carbon films, Science **306**, 666 (2004).

[2] J. N. Coleman *et al.*, Two-dimensional nanosheets produced by liquid exfoliation of layered materials, Science **331**, 568 (2011).

[3] K. I. Bolotin, K. J. Sikes, Z. Jiang, M. Klima, G. Fudenberg, J. Hone, P. Kim, and H. L. Stormer, Ultrahigh electron mobility in suspended graphene, Solid State Commun. **146**, 351 (2008).

[4] H. Tetlow, J. Posthuma de Boer, I. J. Ford, D. D. Vvedensky, J. Coraux, and L. Kantorovich, Growth of epitaxial graphene: Theory and experiment, Phys. Rep. **542**, 195 (2014).

[5] O. V. Yazyev and Y. P. Chen, Polycrystalline graphene and other two-dimensional materials, Nat. Nanotechnol. **9**, 755 (2014).

[6] V. I. Artyukhov, Y. Liu, and B. I. Yakobson, Equilibrium at the edge and atomistic mechanisms of graphene growth, Proc. Natl. Acad. Sci. U.S.A. **109**, 15136 (2012).

[7] Q. Yu *et al.*, Control and characterization of individual grains and grain boundaries in graphene grown by chemical vapour deposition, Nat. Mater. **10**, 443 (2011).

[8] D. Geng, B. Wu, Y. Guo, L. Huang, Y. Xue, J. Chen, G. Yu, L. Jiang, W. Hu, and Y. Liu, Uniform hexagonal graphene flakes and films grown on liquid copper surface, Proc. Natl. Acad. Sci. U.S.A. **109**, 7992 (2012).

[9] Y. Hao *et al.*, The role of surface oxygen in the growth of large single-crystal graphene on copper, Science **342**, 720 (2013).

[10] T. Ma, W. Ren, X. Zhang, Z. Liu, Y. Gao, L.-C. Yin, X.-L. Ma, F. Ding, and H.-M. Cheng, Edge-controlled growth and kinetics of single-crystal graphene domains by chemical vapor deposition, Proc. Natl. Acad. Sci. U.S.A. **110**, 20386 (2013).

[11] J. Chen *et al.*, Near-equilibrium chemical vapor deposition of high-quality single-crystal graphene directly on various dielectric substrates, Adv. Mater. **26**, 1348 (2014).

[12] Y. Liu, S. Bhowmick, and B. I. Yakobson, BN white graphene with "colorful" edges: The energies and morphology, Nano Lett. **11**, 3113 (2011).

[13] Y. Liu, A. Dobrinsky, and B. I. Yakobson, Graphene Edge from Armchair to Zigzag: The Origins of Nanotube Chirality?, Phys. Rev. Lett. **105**, 235502 (2010).

[14] G. Kresse and J. Hafner, Ab Initio molecular dynamics for liquid metals, Phys. Rev. B **47**, 558 (1993); G. Kresse and J. Furthmüller, Efficient iterative schemes for ab initio total-energy calculations using a plane-wave basis set, Phys. Rev. B **54**, 11169 (1996).

[15] P. E. Blöchl, Projector augmented-wave method, Phys. Rev. B **50**, 17953 (1994); G. Kresse and D. Joubert, From ultrasoft pseudopotentials to the projector augmented-wave method Phys. Rev. B **59**, 1758 (1999).

[16] D. M. Ceperley and B. J. Alder, Ground State of the Electron Gas by a Stochastic Method, Phys. Rev. Lett. **45**, 566 (1980).

[17] J. P. Perdew, K. Burke, and M. Ernzerhof, Generalized Gradient Approximation Made Simple, Phys. Rev. Lett. **77**, 3865 (1996); Generalized Gradient Approximation Made Simple, Phys. Rev. Lett. **78**, 1396 (1997).

[18] See Supplemental Material at http://link.aps.org/supplemental/10.1103/PhysRevLett.114.115502 for details of computations and edge energy fitting.

[19] D. J. Klein, Graphitic polymer strips with edge states, Chem. Phys. Lett. **217**, 261 (1994).

[20] P. Wagner, V. V. Ivanovskaya, M. Melle-Franco, B. Humbert, J.-J. Adjizian, P. R. Briddon, and C. P. Ewels, Stable hydrogenated graphene edge types: Normal and reconstructed Klein edges, Phys. Rev. B **88**, 094106 (2013).

[21] L. L. Patera *et al.*, In Situ observations of the atomistic mechanisms of Ni catalyzed low temperature graphene growth, ACS Nano **7**, 7901 (2013).

[22] C. Herring, Some theorems on the free energies of crystal surfaces, Phys. Rev. **82**, 87 (1951).

[23] A. Garcia-Lekue, T. Balashov, M. Olle, G. Ceballos, A. Arnau, P. Gambardella, D. Sanchez-Portal, and A. Mugarza, Spin-Dependent Electron Scattering at Graphene Edges on Ni(111), Phys. Rev. Lett. **112**, 066802 (2014).

[24] M. Olle, G. Ceballos, D. Serrate, and P. Gambardella, Yield and shape selection of graphene nanoislands grown on Ni(111), Nano Lett. **12**, 4431 (2012).

[25] V. I. Artyukhov, E. S. Penev, and B. I. Yakobson, Why nanotubes grow chiral, Nat. Commun. **5**, 4892 (2014).
[26] M. Li, J. B. Hannon, R. M. Tromp, J. Sun, J. Li, V. B. Shenoy, and E. Chason, Equilibrium shape of graphene domains on Ni(111), Phys. Rev. B **88**, 041402 (2013).
[27] J. Lahiri, Y. Lin, P. Bozkurt, I. Oleynik, and M. Batzill, An extended defect in graphene as a metallic wire, Nat. Nanotechnol **5**, 326 (2010).
[28] F. Bianchini, L. L. Patera, M. Peressi, C. Africh, and G. Comelli, Atomic scale identification of coexisting graphene structures on Ni(111), J. Phys. Chem. Lett. **5**, 467 (2014).
[29] After a collision within the same Cu grain the shape of the composite island will approach the original kinematic Wulff construction as it grows larger compared to the separation between the original two. Thus, one could still grow large single crystals with a well-defined shape even starting from more than one nucleus.
[30] A. T. Murdock, A. Koos, T. B. Britton, L. Houben, T. Batten, T. Zhang, A. J. Wilkinson, R. E. Dunin-Borkowski, C. E. Lekka, and N. Grobert, Controlling the orientation, edge geometry, and thickness of chemical vapor deposition graphene, ACS Nano **7**, 1351 (2013).
[31] F. Ding, A. R. Harutyunyan, and B. I. Yakobson, Dislocation theory of chirality-controlled nanotube growth, Proc. Natl. Acad. Sci. U.S.A. **106**, 2506 (2009).
[32] J.-H. Lee *et al.*, Wafer-scale growth of single-crystal monolayer graphene on reusable hydrogen-terminated germanium, Science **344**, 286 (2014).
[33] Y. Ogawa, B. Hu, C. M. Orofeo, M. Tsuji, K.-i. Ikeda, S. Mizuno, H. Hibino, and H. Ago, Domain structure and boundary in single-layer graphene grown on Cu(111) and Cu(100) films, J. Phys. Chem. Lett. **3**, 219 (2012).
[34] A. Ismach *et al.*, Toward the controlled synthesis of hexagonal Boron Nitride films, ACS Nano **6**, 6378 (2012).
[35] K. K. Kim *et al.*, Synthesis of monolayer hexagonal Boron Nitride on Cu foil using chemical vapor deposition, Nano Lett. **12**, 161 (2012).
[36] G. Dong and J. W. M. Frenken, Kinetics of graphene formation on Rh(111) investigated by In Situ scanning tunneling microscopy, ACS Nano **7**, 7028 (2013).
[37] A. M. van der Zande, P. Y. Huang, D. A. Chenet, T. C. Berkelbach, Y. You, G.-H. Lee, T. F. Heinz, D. R. Reichman, D. A. Muller, and J. C. Hone, Grains and grain boundaries in highly crystalline monolayer molybdenum disulphide, Nat. Mater. **12**, 554 (2013).
[38] Y. Zhang *et al.*, Controlled growth of high-quality monolayer WS2 layers on sapphire and imaging its grain boundary, ACS Nano **7**, 8963 (2013).
[39] L. L. Patera, F. Bianchini, G. Troiano, C. Dri, C. Cepek, M. Peressi, C. Africh, and G. Comelli, Temperature-driven changes of the graphene edge structure on Ni(111): Substrate vs hydrogen passivation, Nano Lett. **15**, 56 (2015).
[40] A. Garcia-Lekue, M. Ollé, D. Sanchez-Portal, J. J. Palacios, A. Mugarza, G. Ceballos, and P. Gambardella, Substrate-induced stabilization and reconstruction of zigzag edges in graphene nanoislands on Ni(111), J. Phys. Chem. C, doi:10.1021/jp511069y (2015).
[41] D. Prezzi, D. Eom, K. T. Rim, H. Zhou, S. Xiao, C. Nuckolls, T. F. Heinz, G. W. Flynn and M. S. Hybertsen, Edge structures for nanoscale graphene islands on Co(0001) surfaces, ACS Nano **8**, 5765 (2014).